JJEES

Jordan Journal of Earth and Environmental Sciences

JJEES (2025) 16 (1): 17-27
ISSN 1995-6681

Reservoir Evaluation and Improving Zonation into Flow Units Using the GHE Method, Abu El Gharadig Field, North Western Desert, Egypt

Osama M. Elnaggar[1*], Tamer E. Hamed[2]

[1]Egyptian Petroleum Research Institute, Production Department, Nasr City, Cairo, Egypt
[2]Egyptian Petroleum Research Institute, Exploration Department, Nasr City, Cairo, Egypt

Received on 13 July 2023, Accepted on 23 October 2023

Abstract

A group of sandstone core samples, representing Abu Roash ″E″ Member, was selected from AG-3 well (Abu El Gharadig field) to be evaluated in terms of petrophysics, petrography, XRD, and SEM. Enhancing the reservoir classification into hydraulic units, using (the GHEs) method, was done by creating sub-flow units within the main unit. The limits of different GHEs were determined using the experimental equations of the GHE method. In terms of flow characteristics, the examined samples were differentiated into four main GHEs which are GHE-3, GHE-4, GHE-5, and GHE-6, divided into two sub-units for each. GHE-6B and GHE-3 are the best and worst attributes respectively in terms of flow properties. The new novelty is the differentiation of the samples inside the main unit into sub-units by making new lines (using the equation of this method by adding new different FZI values) that are parallel to the limits of the main flow unit, where samples lie very closely on these lines. Hence sub-units within the main unit could be produced using this new processing, and this leads to a more accurate reservoir description. Petrographically, five microfacies were identified: Calcareous argillaceous quartz arenite, Argillaceous ferruginous quartz arenite, Argillaceous quartz arenite, Glauconitic quartz arenite, and Evaporitic ferruginous quartz arenite. These microfacies involve the main and the branched six GHEs. Diagenetic processes that affected the examined samples are compaction, cementation, replacement, glauconitization, ferrugination, leaching, and dissolution. The X-ray revealed quartz is the main component, in addition to evaporite, iron oxides, iron sulfide and clay minerals in variable amounts. SEM distinguished different pore systems that affect permeability values.

Keywords: *Abu El Gharadig Field; Reservoir Zonation; Petrography, XRD; GHE; North Western Desert*

1. Introduction

Dividing the reservoir into different hydraulic elements or flow units is very important for its assessment in terms of flow properties. The concept of reservoir flow units was examined by many researchers as (Abd El Rahman et al., 2023; Harishidayat et al., 2022; Khalid et al., 2020; Al-Jawad and Saleh, 2020; El Sharawy and Nabawy, 2019; Mohebian et al., 2017; Bear, 2013; Porras and Campos, 2001). Reservoir classification into flow units could be done using different methods as (Martin et al., 1997; Amaefule et al., 1993). Global Hydraulic Elements (GHEs) are another technique (Corbett et al., 2003) to differentiate the hydrocarbon reservoir into a number of GHEs having different relations between porosity and permeability. Even within the same GHE, the capabilities may be varied for the samples of interest, and handling them as a homogenous population is not accurate. So, it is very important to separate the samples within the main GHE into sub-units of different qualities where that will help describe the reservoir more precisely. The study area is located at Abu El Gharadig Basin (Figure 1), which represents one of the main Cretaceous reservoirs in the North Western Desert (Abuseda and El_Sayed, 2022; Farouk et al., 2022a, 2022b, 2022c). The General stratigraphic column of the area of interest is displayed (Fig. 2). Generally, the Cretaceous age was examined by many researchers in Egypt (Sharaka, et al., 2022; El-Desoky et al., 2019; Shalaby et al., 2013; Obaidalla, 2005).

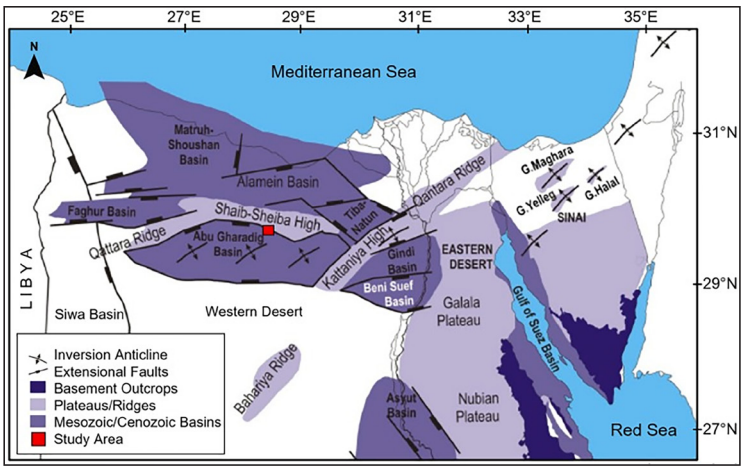

Figure 1. Location map of the study area (Abu El Gharadig field)

* Corresponding author e-mail: osama_221@yahoo.com

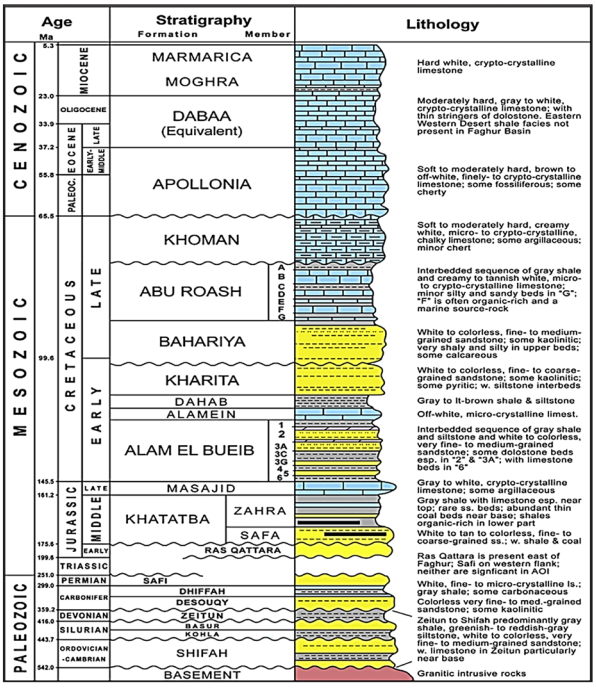

Figure 2. General stratigraphic column of North Western Desert, Egypt (Michael et al. 2016).

Concerning Global Hydraulic elements (GHEs) and for any porosity value, the corresponding permeability could be determined by the next formula:

$$K = \Phi * (((FZI) * (\Phi/1-\Phi)) / 0.0314)^2 \quad (1)$$

where:

K, permeability in mD

φ, porosity in fraction

FZI = flow zone indicator, mm.

There are 10 values of FZI that are already determined by the method of Global Hydraulic Elements (GHEs) which are 0.0938, 0.1875, 0.375, 0.75, 1.5, 3, 6, 12, 24, and 48 for (GHEs) and 1, 2, 3, 4, 5, 6, 7, 8, 9, and 10 respectively. The previous FZI values allow the determination of boundary lines of flow units to cover a wide range of permeability-porosity combination within (GHEs).

2. Study Objectives

The aim of this work is the reservoir evaluation of Abu Roash ″E″ Member, AG-3 well in Abu El Gharadig field in terms of petrophysics, petrography, XRD, and scanning electron microscope. It aims to enhance reservoir zonation into hydraulic units using GHEs method through dividing the main GHE into sub-GHEs of different flow properties. This means more accuracy in deeply investigating the hydrocarbon reservoir in terms of flow units of various capabilities.

The idea of classifying the main GHE into sub-GHE units is done by making new lines (using the equation of this method by adding new different FZI values) that pass through the data points, existing at different levels within the main GHE unit, where these lines/levels are parallel to the main limits or borders of the main GHE unit. Each line represents a subunit within the main GHE.

3. Materials and Methods

In this study, twenty-four available sandstone core samples, representing Abu Roash ″E″ Member, were selected from AG-3 well (Abu El Gharadig field) to be evaluated in terms of petrophysics, petrographic description, X-ray diffraction (XRD), and scanning electron microscope (SEM).

For petrophysical measurements, eighteen-core samples were suitable to be drilled into plugs of diameter 2.5 cm and length 5 cm. Porosity and permeability were measured at the American University of Cairo (soil Lab.), using the methods introduced by (Dakhanova, 1977; Anderson, 1975; Rzhevsky, and Novik, 1971; Kobranova, 1962). Other parameters were calculated from the measured data. We hope that other parameters will be available for deep reservoir investigation in terms of capillary pressure, electrical properties, and pore pressure (Abbey, 2020).

Twenty-four samples were thin-sectioned for petrographic examination. These thin sections were examined under an Olympus microscope in Sedimentary Lab., Egyptian Petroleum Research Institute (EPRI) which is attached to a digital camera to determine the petrographical characteristics and microfacies associations.

Twenty samples are subjected to X-ray diffraction (XRD) to recognize their mineralogy. The analysis was done at the Egyptian Petroleum Research Institute (EPRI) in Central laboratories. Automated powder diffractometer system of Philips type Pan Alytica X- pert- pro was used with Ni- filter, Cu- radiation (1.542= ƛA°) at normal scanning speed 0.02°/S and 40 K.V., 30 m. A. The reflection peaks between 2Ɵ = 4° and 70° were gained for the un-oriented analysis. The identification of the powder samples is determined in semi-quantitative and qualitative analysis. The corresponding relative intensities (I/I°) and d-spacing were gained and correlated with the standard data of ICDD/2010 files using the APD program. The interpretation was done using APD and PDF programs which include powder diffraction and PDf-2 Database sets 1-45.

Three samples of the different lithofacies are micro-photographed, and SEM scanned to realize the microstructure and diagenetic relations in the pore system—main contents and matrix of the examined sediments. Distinguishing the mineral contents, using SEM, is simplified by comparing their morphologic attributes with those displayed in the SEM petrology Atlas (Welton, 1984). SEM was done at the Egyptian Petroleum Research Institute (Central lab.), using a SEM of Philips X L-30 Model that was attached with EDX units, with magnification 10 X up to 400.000 X, resolution for W. (3.5nm) and accelerating voltage 30 K.V. The examined samples were gold coated.

4. Results

4.1 Petrophysics

The petrophysical reservoir properties of the samples of Abu Roash ″E″ Member from AG-3 well are displayed (Table 1). The porosity ranges from 10.9 to 28.3%, where permeability ranges from 1.8 to 90.3 MD. Reservoir quality index (RQI) ranges from 0.1 to 0.73 mm and r35 ranges from 0.65 to 7.37 mm.

Table 1. Petrophysics of the examined samples of Abu Roash ″E″ Member, AG-3 well

S#	Depth, ft	Porosity, %	Permeability, md	RQI, mm	r35, mm
1	9631	28.3	53.2	0.430	3.11
2	9637	21.4	22.4	0.322	2.38
3	9640	19.3	65.2	0.578	4.88
4	9642	25.1	76.3	0.548	4.27
5	9647	14.4	60.3	0.643	6.01
6	9649	10.9	56.9	0.717	7.37
7	9650	13.3	41.3	0.554	5.16
8	9651	26.4	90.3	0.581	4.50
9	9666	16.3	40.2	0.493	4.24
11	9670	15.2	49.4	0.565	5.08
12	9671	22.4	55.3	0.494	3.90
13	9675	16.5	49.9	0.546	4.77
14	9676	19.8	89.3	0.667	5.75
15	9678	14.3	56.4	0.625	5.82
16	9687	17.2	1.8	0.101	0.65
17	9695	14.4	43.3	0.545	4.95
23	9725	16.3	34.7	0.458	3.89
24	9727	11.9	64.6	0.731	7.35

Four main GHEs representing the measured samples are displayed (Figure 3). They are GHE-3, GHE-4, GHE-5, and finally GHE-6. The boundaries of each hydraulic element was constructed according to the equation (1).

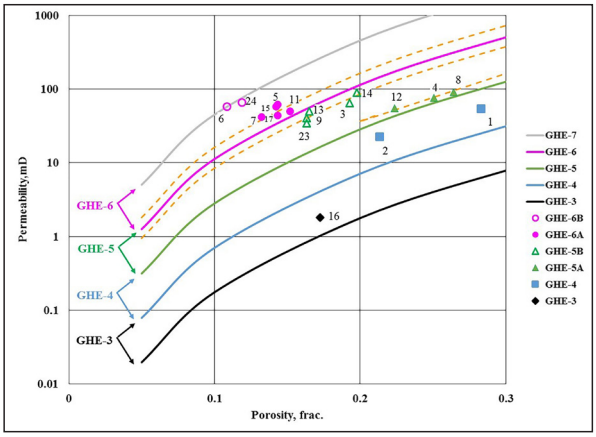

Figure 3. GHEs (main and sub) distribution of the examined samples of Abu Roash ″E″ Member, AG-3 well in the Abu El Gharadig field, (Corbett et al., 2003).

A relation between the Reservoir Quality Index (RQI) and permeability (Figure 4) affirmed the previous results, where the examined samples were distributed in a way similar entirely to that of Figure 3 through parallel trend lines.

Another relation was constructed (Figure 5), using the calculated r35 to display the hydraulic capabilities of the examined samples. The examined samples were distinguished into two groups, the mesoport flow unit, where r35 ranges from 0.5 to 2.0 mm, and the macroport unit, where r35 ranges from 2.0 to 10.0 mm (Martin et al., 1997).

The calculated pore size distribution (Figure 6) was constructed, using empirical calculations (Pittman, 1992) to define the available pore throat radii (μm) within the samples of interest that agree with different saturation percent of mercury (10-75%).

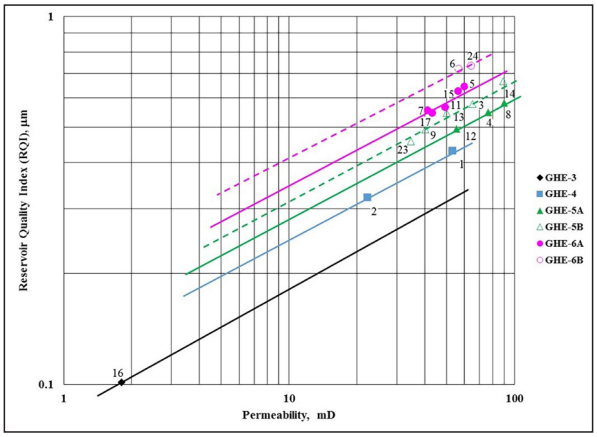

Figure 4. Reservoir quality index (RQI) versus permeability of the examined samples of Abu Roash ″E″ Member, AG-3 well in Abu El Gharadig field.

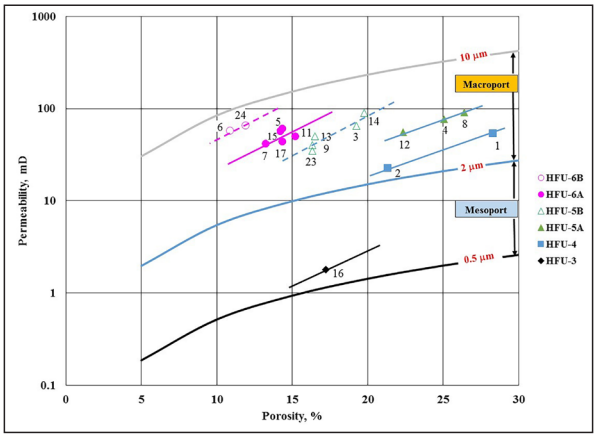

Figure 5. Flow unit distribution of the examined samples using r35 of the examined samples of Abu Roash ″E″ Member, AG-3 well in Abu El Gharadig field.

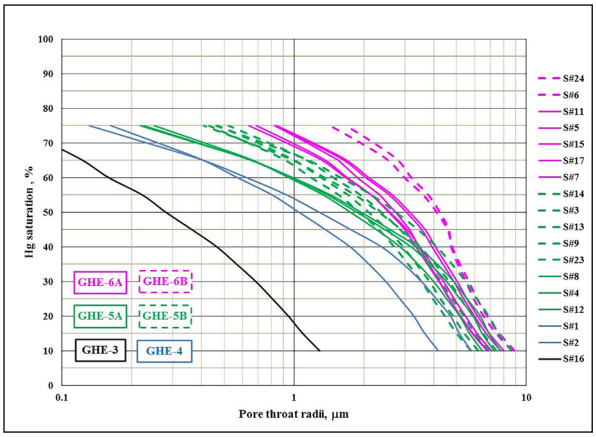

Figure 6. Calculated pore size distribution of the examined samples of Abu Roash ″E″ Member, AG-3 well in Abu El Gharadig field.

4.2 Petrography

The classification of microfacies is used for their simplicity, and they are based on characteristics that are easily determined under the microscope. The study was carried out on twenty-four prepared thin sections representing all the study samples of ″E″ Member in AG-3 well to illustrate their constituents. The petrographic description of the clastic rocks showed the next microfacies types (Plate 1). The depositional environment of clastic samples is determined here according to (Scholle and Spearing, 1982).

4.2.1. Calcareous Argillaceous Quartz Arenite

It is recorded in Abu Roash ″E″ Member from the depth of 9631 to 9647 ft, (S#1-5). This microfacies type, plate 1(B&C), is medium to coarse, sub-angular to sub-rounded detrital quartz grains (92%) and nearly (5%) clay matrix, carbonate, and cement (3%). Quartz grains are moderately to well sorted and most grains are of monocrystalline type with some polycrystalline grains, where they range from sub-mature to mature.

4.2.2. Argillaceous Ferruginous Quartz Arenite

This microfacies type exists in middle part of ″E″ Member from the depth of 9671 to 9676 ft, (S#12-14). It is medium to coarse sand size, moderately to well sorted, sub-angular to sub-rounded detrital quartz grains (about 87%) with some iron oxide fundamentally hematite nearly (7%) and about (5%) clay matrix (Plate1-D). Some of these quartz grains are mostly monocrystalline, where few are polycrystalline. Quartz grains are cemented by carbonate mainly (sparry calcite crystals) about (1%).

4.2.3. Argillaceous Quartz Arenite

This microfacies is recorded in Abu Roash ″E″ Member from the depth of 9678 to 9706 ft, (S#15-19). This microfacies is medium to coarse, sub-angular to sub-rounded detrital quartz grains (95%) and nearly (5%) clay matrix, evaporites, carbonate, and iron oxide cement (Plate1-A). Texturally, quartz grains are moderately to well sorted, and most grains of monocrystalline with some polycrystalline grains. They range from sub-mature to mature.

4.2.4. Glauconitic Quartz Arenite

This sandstone microfacies exists in Abu Roash ″E″ Member from 9710 to 9727 ft, (S#20-24). It is coarse to medium, sub-rounded to sub-angular, monocrystalline, moderately sorted, detrital quartz grains of sub-mature nature forming about (89%) of the rock and iron oxide (1%) cemented by argillaceous matrix. Glaucontization is shown as scattered grains about (7%) forming or peloids, rounded to sub-rounded, green-colored, may be formed from pre-existing clay minerals and/or by the presence of decaying matter (Plate1-F).

4.2.5. Evaporitic Ferruginous Quartz Arenite

This microfacies is recorded in Abu Roash ″E″ Member at depth from 9649 to 9670 ft, (S#6-11). It is medium to fine, sub-rounded to sub-angular, moderately sorted, sub-mature detrital quartz grains (86%), and iron oxide mainly Hematite (8%). A little amount of evaporites mainly halite (4%) and argillaceous matrix can be shown (2%). The intergranular porosity is filled mostly with iron oxide cement mainly hematite and goethite (Plate1-E). Microfacies of the examined samples and equivalent GHEs/Sub-GHEs is displayed (Table 2), where sample distribution within these microfacies is shown (Table 3). The distribution of microfacies along the depth of the examined samples is displayed (Figure 7).

Table 2. Microfacies of the examined samples and equivalent GHEs/Sub-GHEs

Microfacies	Involved samples	Representative plate	Equivalent GHEs (main/sub)
Calcareous argillaceous quartz arenite	S#1-5	Plate1 (B&C)	GHE-4, S#1,2 GHE-5B, S#3 GHE-5A, S#4 GHE-6A, S#5 GHE-6A, s#5
Argillaceous ferruginous quartz arenite	S#12-14	Plate1-D	GHE-5A, S#12 GHE-5B, S#13,14
Argillaceous quartz arenite	S#15-19	Plate1-A	GHE-6A, S#15,17 GHE-3, S#16
Glauconitic quartz arenite	S#20-24	Plate1-F	GHE-5B, S#23 GHE-6B, S#24
Evaporitic ferruginous quartz arenite	S#6-11	Plate1-E	GHE-6A, S#7&11 GHE-6B, S#6

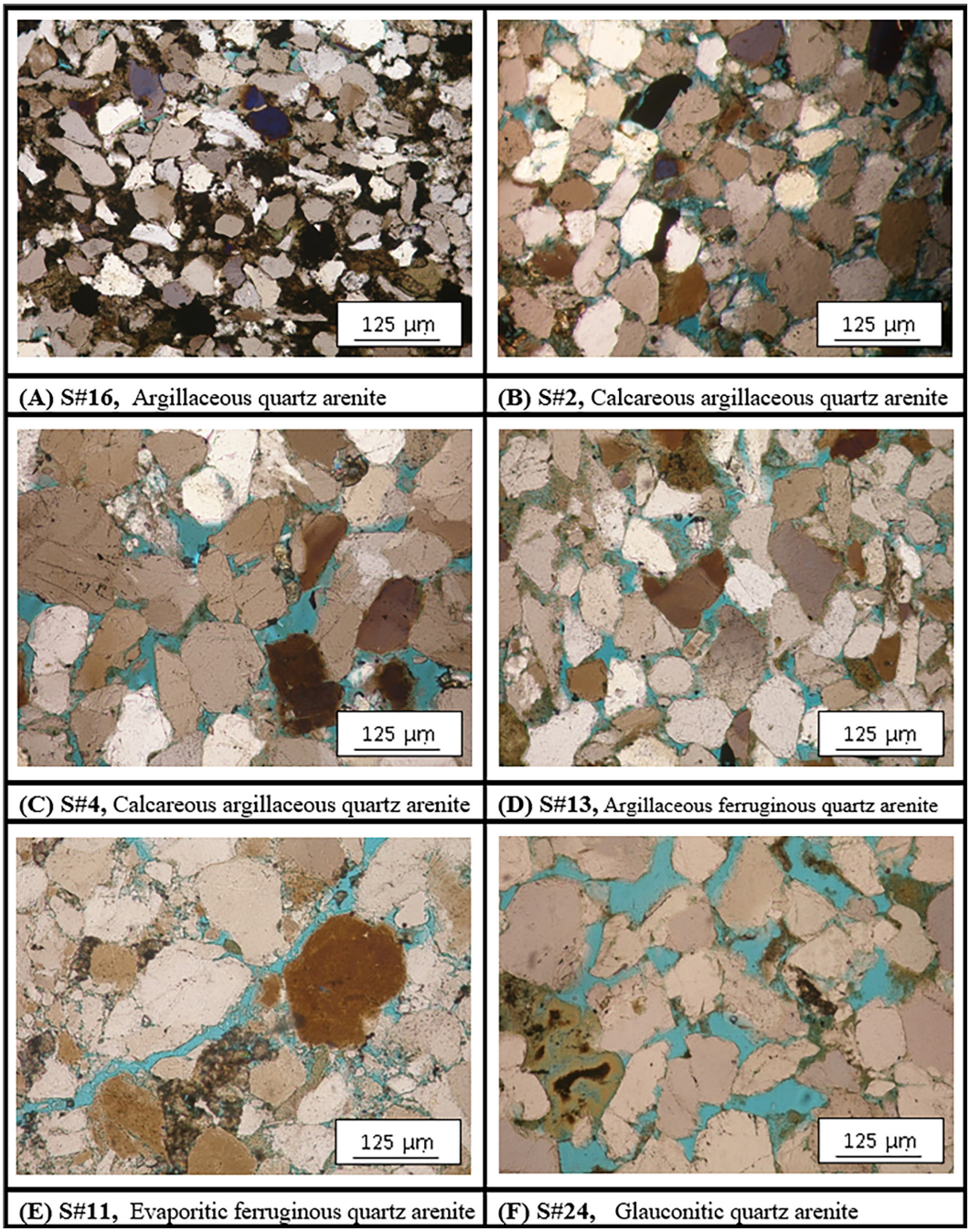

Plate 1. Microfacies of the examined samples of Abu Roash "E" Member, AG-3 well in Abu El Gharadig field.

Table 3. Main/sub GHEs and equivalent microfacies of the examined samples

Main GHE	Involved samples	Sub-GHE with samples	Microfacies	Plate
GHE-3	16	None	Argillaceous quartz arenite	Plate1-A
GHE-4	1, 2	None	Calcareous argillaceous quartz arenite	Plate1 (B&C)
GHE-5	8, 4, 12, 14, 3, 13, 9, 23	GHE-5A: 4, 8, 12	Calcareous argillaceous quartz arenite, S#4	Plate1-(B&C)
			Argillaceous ferruginous quartz arenite, S#12	Plate1-D
		GHE-5B: 3, 9, 13, 14, 23	Calcareous argillaceous quartz arenite, S#3	Plate1 (B&C)
			Argillaceous ferruginous quartz arenite, S#13	Plate1-D
			Glauconitic quartz arenite, S#23	Plate1-F
GHE-6	11, 5, 15, 17, 7, 24, 6	GHE-6A: 5, 7, 11, 15, 17	Calcareous argillaceous quartz arenite, S#5	Plate1 (B&C)
			Evaporitic ferruginous quartz arenite, S#7,11	Plate1-E
			Argillaceous quartz arenite, S#15,17	Plate1-A
		GHE-6B: 6, 24	Evaporitic ferruginous quartz arenite, S#6 Glauconitic quartz arenite, S#24	Plate1-E Plate1-F

4.3 Diagenetic Processes of Sandstones

The effects of diagenetic processes occurred in sandstones have been reported and classified by many researchers from different parts of the world, such as (Qian et al., 2022; Qian et al., 2020a & 2020b; Wang et al., 2020; Biorlykke and Ehrenberg, 1993; Moraes and De Ros, 1992). The petrographic investigation of thin sections displays the following main diagenetic features identified from the examined sandstone microfacies:

4.3.1. Compaction (Pressure Solution)

Mechanical compaction including dewatering, deformation, and re-orientation of grains. Chemical compaction is dissolution mainly along surfaces such as stylolite or solution seams. Compaction can lower porosity up to 40% or more and in some cases does an important function in porosity reduction than cementation (McBride et al., 1996).

4.3.2. Cementation

Cementation in clastic sediments is an essential diagenetic operation leading to solidification of the loose detrital sediments into rocks by deposition of minerals from the interstitial fluids and/or forming minerals in authigenic forms. It depends on temperature, pressure, framework assemblage composition, solute composition, pore water composition, and time (Wood, 1989). Cementation is one of the most porosity-reducing operations (Hayes, 1979).

4.3.3. Replacement

This operation includes the decay of the original minerals and the evolution of replacing minerals crystals as cement in both pre-existing and formed void space (Blatt et al., 1972). Generally, ferruginous cemented sandstone may be formed through siderite oxidation (Pettijohn, 1975). Most of the hematite and its precursor oxides (goethite) in sandstones were formed in situ after precipitation through the intrastratal alteration of iron-bearing minerals in hot arid or semi-arid climates or desert basins (Turner, 1980; Walker et al., 1978). The forming of iron oxides (goethite and hematite) is brought about by the development of well-drained oxygenated conditions and the seasonal lowering of water tables, allowing the organic matter oxidation (Selley, 1996; Besly and Turner, 1983). Iron oxides formation as cement or matrix in intergranular pore system of the study samples does an important role in porosity reduction.

4.3.4. Glauconitization

Glauconitization is noticed as peloids or scattered grains, sub-rounded to rounded, green in color, perhaps formed in warm water (15-200 Co) from pre-existing clay minerals at depth ranges from 400 up to 3000 m at pH 7-8, (Plate1-F).

4.3.5. Ferrugination

Pettijohn (1975) proposed that ferruginous cemented sandstones at most may be originated through the siderite oxidation. Selley (1996) and Besly and Turner (1983) considered that the iron oxides formation (hematite and goethite) beds happened through the development of well-drained oxygenated conditions and seasonal lowering of water tables, allowing the organic matter oxidation (Plate-1-B). Turner (1980) and Walker et al. (1978) proposed that hematite and its precursor oxides (mainly goethite) in sandstones at most, were originated in situ after deposition by the interstratal alteration of iron bearing minerals in semi-arid or hot arid climates or desert basin.

4.3.6. Leaching

The leaching diagenetic process in the examined sandstone rock samples is presented in (Plate1-A).

4.3.7. Dissolution

The early diagenetic operation of examined sandstones involves the dissolution of certain frameworks of specific minerals such as quartz. Dissolution in clastic rocks was recorded as a significant diagenetic appearance for boosting secondary porosity (Lundegard et al., 1984) and increment mineral maturity (Abd El-Wahab and McBride, 1991), in addition to texture maturity (Walker et al., 1978). The dissolution process is a very significant diagenetic agent for characterizing the reservoir rock, which improves the porosity and permeability (Selley, 1998). Displaying authigenic mineral or grain dissolution can improve the porosity as a secondary type (Ehrenberg, 1990). The acidic solution may affect quartz grains during the late stage to be etched and corroded to produce grains of irregular shapes, Plate1 (E&F).

4.4 Mineralogy (XRD)

The mineralogical bulk analysis of the examined samples was completed by the X-ray diffraction analysis (XRD) alongside the Scanning Electron Microscopy (SEM). They were used for detection of the main and minor minerals. Recognizing the mineralogical content of the examined samples can be easily detected through using the X-ray diffraction technique (XRD). The X-ray diffraction analysis is an important technique due to its active function in the field of petrography and mineralogy. Chilingar et al. (1967) pointed out that usage of X-ray diffraction analysis would make it possible to distinguish between formations having the same age as well as between different rock units of different ages.

The aim of this study also determines the mineralogical composition varieties of the rocks in the examined well, hence defining the environmental condition. The mineralogy of the twenty-four examined samples were determined by the use of X-ray diffractometer (XRD). Each sample was ground to powder, and 0.5 g. portion of the ground material was pressed into a coveter 10 mm in diameter. This pressed material was analyzed to determine the whole bulk rock mineralogical composition.

4.4.1. Mineralogical Composition of the Bulk Samples

The identification of mineralogy from bulk composition of the ″E″ Member samples was obtained from X-ray results and was explained using cards of American Society for Testing Materials (ASTM) with published data by Deer et al. (1963)and Brown (1961). The results of X-ray diffraction revealed presence of quartz as the main component, in addition to evaporate, iron sulfide, iron oxides and clay minerals in variable amounts and minor calcite.

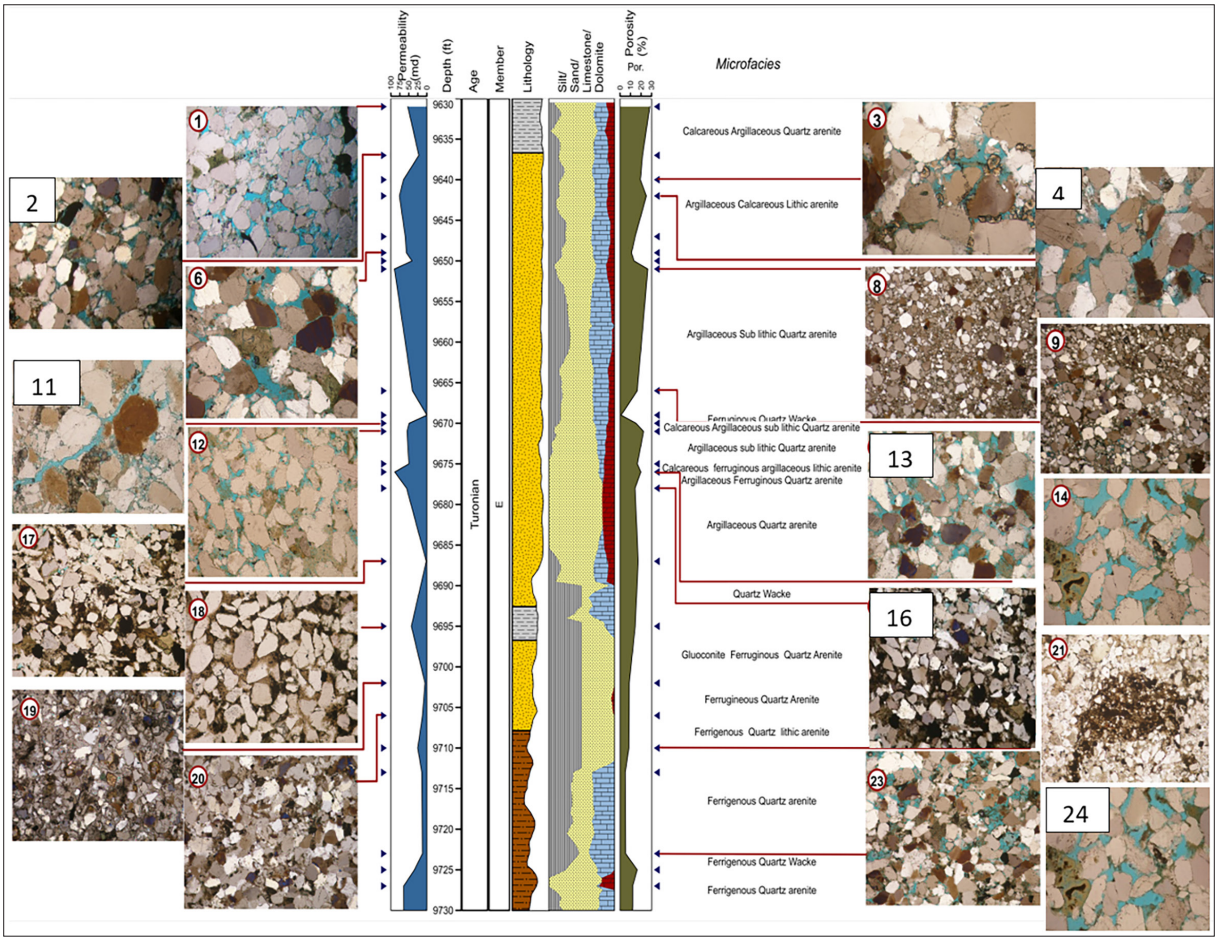

Figure 7. The distribution of microfacies of the examined samples of Abu Roash ″E″ Member, AG-3 well in Abu El Gharadig field.

4.4.2. Quartz

Quartz is the most abundant clastic mineral in the bulk samples. It can be identified at X-ray reflections 4.24 A0, 3.34 A0, and 1.82 A0 that coincide with the ASTM card No. 5-0490. The microscopic check of non-carbonate samples detected the presence of quartz as detrital grains, Plate (2).

4.4.3. Halite

Halite is recorded as a minor mineral in these samples such as S#4 (Plate2-C). Halite can be identified at reflection 2.82 A°, 1.99 A° and 1.62 A° coincide with ASTM card No. 5-0628.

4.4.4. Iron Sulfide (Pyrite)

Pyrite was discovered in the Abu Roash ″E″ Member in most samples. It was recognized in the diffractograms by its characteristic lines at 1.63 A°, 2.71 A°, and 2.42 A° that coincide with ASTM card No. 04-008-7762. The existing of pyrite in ″E″ Member indicates the spread of a reducing environment during its deposition. Pyrite is formed in sediments as a consequence of the bacterial reduction of seawater sulfate (Berner, 1982). The pyrite is also recorded in some samples, Plate2 (A-F) exist in vast quantities in numerous states of crystallization such as rhombs, framboids and specks.

4.4.5. Iron Oxides (Hematite)

The deposition of Fe2O3 in marine environments requires a lower Eh & pH, and being favorable in an oxidizing carbonic acid zone. Hematite is identified using X-ray reflections 3.69 A°, 2.69 A° and 2.51 A°, which coincide with ASTM card No. 33-664, plate2 (A&D). Generally, iron oxides occur in many different phases authigenic iron oxide in the form of hematite and detrital iron oxide as grain coating and scattered interstitial matrix, in clay structure and as iron oxide film on clay surface. The soluble of iron in hydrothermal solutions began precipitate due to change in their pH and Eh and also due to decrease in the temperature of the solution. Oxidizing Fe++ is more complete at relatively high pH solutions.

4.4.6. Clay Minerals (Montmorillonite)

Montmorillonite is identified by basal reflection 15.01A°, 5.01A°, and 3.56A° using ASTM card No. 14-164, Plate2 (A, C, D&E). Krauskopf (1979 documented that the montmorillonite formed from the weathering of intermediate to calc-mafic rocks including volcanic ash. Montmorillonite is originated from soil with relatively high pH, rich in Ca+2, and Mg+2 and under impeded drainage (Mohr et al., 1971). It can also be formed as post-depositional diagenesis of degraded micas by water of low ionic strength running through porous rocks (Velde and Nicot, 1985).

4.4.7. Carbonate Minerals

Calcite is the minor carbonate minerals in bulk sandstone samples, plate2 (C&D). Calcite can be identified at reflections 3.85 A0, 3.03 A0 and 2.09 A0 that coincide with ASTM card No. 5-0586.

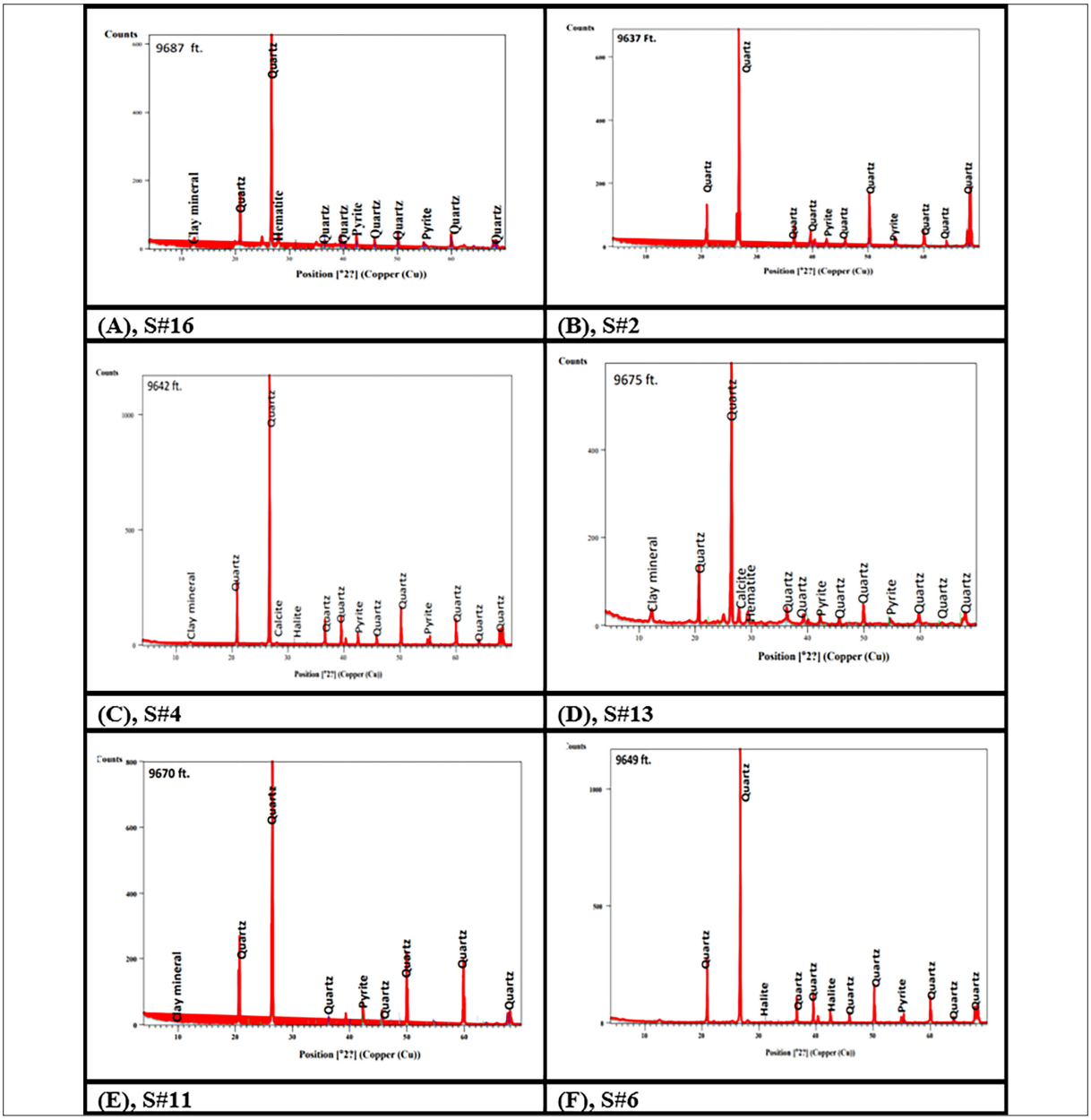

Plate 2. Bulk X- ray diffraction charts of some representative samples of Abu Roash ″E″ Member, AG-3 well in Abu El Gharadig field.

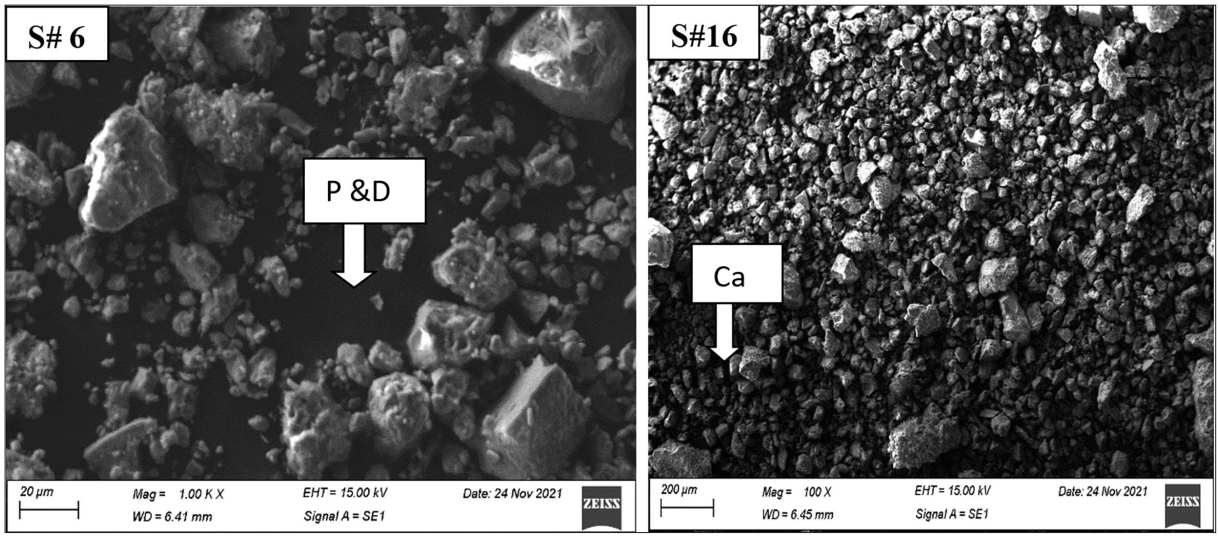

Figure 8. SEM showing quartz arenite of samples (6&16) with pore geometry, dissolution diagenetically and calcite cement, Abu Roash ″E″ Member, AG-3 well in Abu El Gharadig field.

P: Pore geometry. D: Dissolution. Ca: Cementation with calcite.

4.5. Scanning Electron Microscope (SEM) and (EDX).

The petrographic study, when integrated with SEM investigations, supplies a good way to identify the mineralogical features and the diagenetic processes that affect the rock forming minerals (Mousa et al., 2009; Khalil et al., 1999). The next SEM and EDX study was used to clarify and recognize the authigenic minerals, pore geometry (Figure 8), and diagenetic events which are produced by various environments for the examined quartz at Abu Roash ″E″ Member in Cretaceous rock units. The identified microfacies association was deposited in moderately agitated districted from tidal flat beach environments to bank margins (Flugel, 2010 and 2004).

5. Discussion

The new addition of this study as we mentioned previously is making new sub-units within the main GHE. The new sub-units (Figure 3) were found in GHE-5 and GHE-6 with different symbols for each new sub-GHE. GHE-5 involves (GHE-5A & GHE-5B), whereas GHE-6 involves (GHE-6A & GHE-6B). The differentiation of the whole samples within the main GHE into a number of sub-GHEs makes the reservoir description more accurate than before. Table 2 displays the samples of each main and branched GHE.

A number of relationships confirmed the sample differentiation into hydraulic groups as Figure (3), as the relation between Reservoir Quality Index (RQI) and permeability (Fig. 4) illustrates the flow units distribution of the examined samples using r35 of the examined samples of Abu Roash ″E″ Member, AG-3 well in Abu El Gharadig field. Figure 5 displays the macro-port flow unit comprising the samples of GHE-4, GHE-5, and GHE-6 of Figure 3, where the examined samples (GHE-5 and GHE-6) have been differentiated in a way (the trend lines) that reflects the sub-GHEs of Figure 3. Finally, the calculated pore size distributions (PSD) were separated into different groups (Figure. 6) that assured the presence of the sub-flow units of Figure 3.

Petrographically, the depositional environments of microfacies types of the examinedexamined clastic samples were characterized by shallow marine conditions of the intertidal zone for Calcareous argillaceous quartz arenite, intertidal conditions for Argillaceous ferruginous quartz arenite, shallow marine conditions of the intertidal zone for Argillaceous quartz arenite, shallow marine intertidal conditions for Glauconitic quartz arenite, and finally shallow marine intertidal conditions for Evaporitic ferruginous quartz arenite.

Concerning the diagenetic processes of the examined samples, the effect of compaction gives (secondary porosity) overburden pressure as shown in Plate1 (A & E) during the middle stage, and it is shown in (Plate1-A) at a late stage of diagenetic processes. Cementation is represented by three kinds in the examined samples: The first is calcite (Plate-1B) during the early stage, the second is evaporites as shown in (Plate-1A), finally, by iron oxides as shown in Plate-1 (A, B &F) & Plate-2 (A&D). Hematite is the latest authigenic mineral in the examinedexamined sandstone. It occurs as rims on quartz grains that are commonly preserved between quartz grains and represent the later authigenic phases. Iron could be provided by intrastratal ferrosilicate solution from the clay beds in the examinedexamined section since the diagenetic environment was oxidizing.

Petrographical check showed the occurrence of iron minerals (hematite) as a cement replacing mineral in sandstone samples in Plate-1 (A&E).

The glauconite formation is facilitated with existing of decayed organic matter (Plate1-F). Leaching process (Plate1-A) is indicated by presence of oversize pores. These pores are formed by dissolving out or selective removal of the intergranular silicate minerals. This is the main diagenetic process to make high porosity during the late stage.

Mineralogy determination using X-ray diffraction analysis (XRD) helped determine the environmental conditions. SEM (Figure 8) distinguished different pore systems that can affect permeability values. The wider pore spaces are obvious for sample (6) which is the permeable one (56.9 mD), where the narrower pore spaces are clear for sample (16) that is the tight one (1.8 mD), also calcite cement was detected for sample#4 (Figure 9).

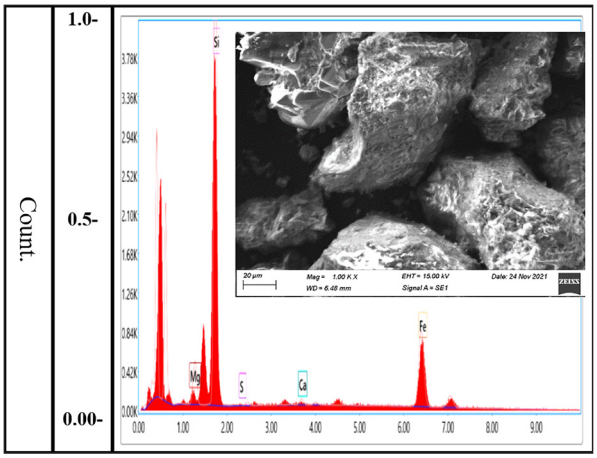

Figure 9. EDX and SEM showing calcite cement and replacement by iron oxide in Calereous quartz arenite microfacies, S#4, Abu Roash ″E″ Member, AG-3 well in Abu El Gharadig field.

6. Conclusion

The examinedexamined samples were classified into four zones of GHEs (GHE-3, GHE-4, GHE-5, and GHE-6). The new processing with GHE method permits adding sub-GHE flow units that enable better understanding of petroleum reservoir, where GHE-5 and GHE-6 were divided into two sub-units for each. The GHE method gives more details about flow units than r35 method. The effect of hematite in reducing the flow properties is obvious on GHE-3 unit. GHE-6B represents the best flow units where GHE-3 unit is the worst. Pore system similarity makes the samples have the same flow properties although they belong to different microfacies as in GHE-5 and GHE-6 flow units. SEM shows the positive/negative effects of pore geometry on the permeability values of the rocks. The results show that a specific microfacies can comprise several different reservoir flow units. Contrarily, similar flow units could be related to different microfacies.

Acknowledgments

The authors would like to thank Khalda Petroleum Company and General Egyptian Petroleum Corporation (E.G.P.C) for supplying the data required to achieve this study.

References

Abbey, C., Oniku, A., Meludu, C., Sebastian, A. (2020). Rock physics analysis of abnormal pore pressure regime offshore Niger Delta Basin. Jordan Journal of Earth and Environmental Sciences, 11: 224-233.

Abd El Rahman, A.A., Elnaggar, O.M., Mohamed, S.F. (2023). Magnetic susceptibility as an indication of reservoir properties of the Nubia Group in Aswan-Komombo, Southern Egypt. Egyptian Journal of Petroleum 32: 31-41.

Abd El-Wahab, A.A., and McBride, E.F. (1991). Digenetic control or reservoir quality of Araba and aqua diagenetic quartz arenites (Cambrian), Gebel Araba-Qabeliat, Southwest Sinai, Egypt. Egyptian Delta Journal of Science 15: 160-203.

Abuseda, H., and El_Sayed, A. M. (2022). Petrographical and petrophysical studies of some Upper Cretaceous rocks, Western Desert, Egypt. Jordan Journal of Earth and Environmental Sciences 13: 37-47.

Al-Jawad, S.N., and Saleh, A.H. (2020). Flow units and rock type for reservoir characterization in carbonate reservoir: case study, south of Iraq. Journal of Petroleum Exploration Production Technology 10: 1-20.

Amaefule, J.O., Altunbay, M., Tiab, D., Kersey, D., Keelan, D.K. (1993). Enhanced reservoir description, using core and log data to identify hydraulic (flow) units and predict permeability in un-cored interval wells SPE-26436. Society of petroleum engineers Conference, Houston, Taxes, U. S. A., 3-6 October, pp. 94-135.

Anderson, G. (1975). Coring and core analysis handbook, Petroleum Publishing Company. Tusla.

Bear, J. (2013). Dynamics of fluids in porous media. Courier Corporation, Chelmsford.

Berner, R.A. (1982). Burial of organic carbon and pyrite sulfur in the modern ocean: its geochemical and environmental significance, American Journal of Science 282: 451-473.

Besly, Y.B., and Turner, P. (1983). Origin of red beds in a moist tropical climate (Etruria Formation, Upper Carboniferous, UK). In: Wilson, R.C. (ed.) Residual Deposits: Surface Related Weathering Processes and Materials. Geological Society London Special publications 11: 131-147.

Biorlykke, K., and Ehrenberg, P.K. (1993). Quartz cementation in sedimentary basins. American Association of Petroleum Geologists Bulletin 77: 1538-1548.

Blatt, H., Middleton, G., Murray, R. (1972). Origin of sedimentary rocks. 2nd edition. Prentice Hall, Inc., Englewood Cliffs, New Jersey. U.S.A.

Brown, C. (1961). The X-Ray identification and crystal structure of clay minerals. A symposium, the Mineralogical Society, London, p. 544.

Chilingar, G.V., Bissel, H.J., Fairbridge, R.W. (1967). Carbonate rocks: origin occurrence and classification developments in sedimentology. Elsevier, publ. Co. London, New York.

Corbett, P.W.M., Ellabard, Y., Mohhammed, K. (2003). Global Hydraulic Elements-Elementary Petrophysics for Reduced Reservoir Modeling. EAGE 65th Conference and Exhibition.

Dakhanova, N.V. (1977). Determination of the petrophysical characteristics of sample. Russian, Nedra, Moscow, p. 41.

Deer, W., Howie, R.A., Zssman, J. (1963). Rock-forming minerals. John Willey and Sons, New York, comprehensive treatise, with excellent coverage on chemistry, crystal structure and paragenesis 5: 1788.

Ehrenberg, S.N. (1990). Relationship between diagenesis and reservoir quality in sandstones of the Garn Formation, Haltenbanken, mid-Norwegian continental shelf. American Association of Petroleum Geologists Bulletin 74: 1538-1558.

El-Desoky, H., Farouk, S., Heikal M., El-Mahallawy, M., Wahid, A. (2019). Geochemical and technical investigation of some clay materials in the Bahariya Oasis, Western Desert, Egypt: Implication in the vitrified clay pipes Industry. Journal of African Earth Sciences 160: 103612.

El Sharawy, M.S., and Nabawy, B.S. (2019). Integration of Electrofacies and Hydraulic Flow Units to Delineate Reservoir Quality in Uncored Reservoirs: A Case Study, Nubia Sandstone Reservoir, Gulf of Suez, Egypt. Natural Resources Research 28: 1587-1608.

Farouk, S., Sen, S., Abu-Alam, T., Al Kahtany, K. (2022a). Geomechanical assessment of the Lower Turonian AR-F limestone Member, Abu Gharadig Field, Egypt: Implications for unconventional resource development. Frontiers in Earth Science 10.

Farouk, S., Sen, S., Abuseda, H., El-Shamly, Y., Salam, A., Elhossainy, M.M. (2022b). Petrophysical Characterization of the Turonian and Cenomanian Intervals in the Abu Gharadig Field, Western Desert, Egypt: Inferences on Reservoir Quality and Resource Development. Natural Resources Research 31: 1793-1824.

Farouk, S., Sen, S., Ganguli, S.S., Ahmad, F., Abioui, M., Al-Kahtany, K., Gupta, P. (2022c). An integrated petrographical, petrophysical and organic geochemical characterization of the Lower Turonian Abu Roash-F carbonates, Abu Gharadig field, Egypt-Inferences on self-sourced unconventional reservoir potential. Marine and Petroleum Geology 145: 105885.

Flugel, E. (2004). Microfacies of carbonate rocks analysis, 1st interpretation and application Springer-verlag, Berlin Heideberg, Newyork. p. 956.

Flugel, E. (2010). Microfacies of carbonate rocks analysis, 2nd interpretation and application Springer-verlag, Berlin Heideberg, Newyork. P. 1006.

Harishidayat, D., Farouk, S., Abioui, M. and Aziz, O.A. (2022). Subsurface Fluid Flow Feature as Hydrocarbon Indicator in the Alamein Basin, Onshore Egypt; Seismic Attribute Perspective. Energies 15: 1-16.

Hayes, J.B. (1979). Sandstone diagenesis, the hole truth. S. E. P. M., Spec. publ., 26: 127-139

Khalid, M., Desouky, S.D., Rashed, M., Shazly, T., Sediek, K. (2020). Application of hydraulic flow units' approach for improving reservoir characterization and predicting permeability. Journal of Petroleum Exploration and Production Technology 10: 467-479.

Khalil, S.M., El-Baz, M.H., Abu-Assy, E.M. (1999). Petrography and diagenesis of Gabal El-Khashab. Red Sea, Egyptian Journal of Geology 5: 119-133.

Kobranova, V.N. (1962). Physical properties of rocks. In Russian Gestopechizdat, Moscow, p. 490.

Krauskopf, K.B. (1979). Introduction to Geochemistry, Mc, Graw-Hill, New York.

Lundegard, P.D., Land, L.S., Galloway, W.E. (1984). Problem of secondary porosity: Frio Formation (Oligocene), Texas Gulf Coast. Geology 12: 399-402.

Martin, A.J., Solomon, S.T., Hartmann, D.J (1997). Characterization of petrophysical flow units in carbonate reservoirs. American Association of Petroleum Geologists Bulletin 81: 734-759.

McBride, E.F., Abdel-Wahab, A.A., Salem, A.M.K. (1996). Influence of diagenesis on reservoir quality of Cambrian and Carboniferous sandstones, southwest Sinai, Egypt. Journal of African Earth Sciences 22: 285-300.

Michael, A.A., Matthias, D.G., James, W.C., Melissa, T. (2016). Egypt far Western Desert basins petroleum charge system as defined by oil chemistry and unmixing analysis. Marine and Petroleum Geology 77: 54-74.

Mohebian, R., Riahi, M.A., Kadkhodaie, A. (2017). Characterization of hydraulic flow units from seismic attributes and well data based on a new fuzzy procedure using ANFIS and FCM algorithms, example from an Iranian carbonate reservoir. Carbonates and Evaporites 34: 349-358.

Mohr, E.C.J., Van Baren, F.A., Van Schuylenborgh, J. (1971). Tropical soils, The Hague, the Netherland, In: Seghal et al., (1974), Genesis transformation and classification of clay minerals in Bulletin-Indian Society of Soil Science 9: 1-21.

Moraes, A.S., and De Ros, L.F. (1992). Depositional infiltrated and authigenic clays in fluvial sandstone of the Jurassic Sergio Formation. Reconocovo Basin, Northeastern Brazil, S.E.P.M. Special Publication 47: 197-208.

Mousa, A.S., El-Hariri, T.Y.M., El-Meligy, W.M. (2009). Assessing the influence of diagenetic processes at El-Gedida Mines, El- Bahariya Oasis, Egypt. Australian Journal of Basic and Applied Sciences 3: 1749-1762.

Obaidalla, N.A., (2005). Complete Cretaceous/Paleogene (K/P) boundary section at Wadi Nukhul, southwestern Sinai, Egypt: inference from planktic foraminiferal biostratigraphy. Rev. de Paléobiol., Gen. 24: 201-224.

Pettijohn, F.J. (1975). Sedimentary rocks. Harper and Row New York, 3rd ed.

Pittman, E.D. (1992), Relationship of porosity and permeability to various parameters derived from mercury injection-capillary pressure curves for sandstone. American Association of Petroleum Geologists Bulletin 76: 191-198.

Porras, J.C., and Campos, O. (2001). Rock typing: a key approach for petrophysical characterization and definition of flow units, Santa Barbara Field. Eastern Venezuela Basin. Presented at the SPE Latin American and Caribbean Petroleum Engineering Conference, Buenos Aires, Argentina, 25-28 March. Paper SPE-69458-MS.

Qian, W., Sun, Q., Jones, S.J., Yin, T., Zhang, C., Xu, G., Zhang, B. (2022). Diagenesis and controlling factors of Oligocene Huagang Formation tight sandstone reservoir in the south of Xihu sag, the East China Sea Shelf Basin. Journal of Petroleum Science and Engineering 215: 110579.

Qian, W., Yin, T., Zhang, C., Hou, G., He, M. (2020a). Diagenesis and diagenetic stages prediction of Ed2 reservoir in the west of Bozhong sag. Petroleum 6: 23-30.

Qian, W., Yin, T., Zhang, C., Tang, H., Hou, G. (2020b). Diagenetic evolution of the Oligocene Huagang Formation in Xihu sag, the East China Sea Shelf Basin. Scientific report 10: 19402.

Rzhevsky, Y., and Novik, G. (1971). The physics of rocks. Translation and Edited by A. A. Beknazarov, Mir publishers, Moscow, p. 320.

Scholle, P.A., and Spearing, D. (1982). Sandstone depositional environment. American Association of Petroleum Geologists Bulletin, Memoir 31. Tulsa, Oklahoma, U.S.A., pp. 1-320.

Selley, R.C. (1998). Elements of Petroleum Geology (2nd), Academic Press limited: California, USA.

Selley, R.C. (1996). Ancient sedimentary environments and their subsurface diagnosis. 4th edition, London.

Shalaby, M.R., Hakimi, M.H., Abdullah, W.H. (2013). Modeling of gas generation from the Alam El-Bueib formation in the Shoushan Basin, northern Western Desert of Egypt. International Journal of Earth Sciences 102: 319-332.

Sharaka, H. K., El-Desoky, H. M., Abd El-Moghny, M. W., Hafez, N. A. A., Abuelleban, S. A. (2022). Geological, Mineralogical and Physical Properties of Aswan Kaolinitic Clays, Egypt: Implications for Industrial Applications. Jordan Journal of Earth and Environmental Sciences 13: 64-73.

Turner, P. (1980). Continental Red Beds: Development in Sedimentology. Elsevier, Amsterdam.

Velde, B., and Nicot, E. (1985). Diagenetic clay mineral composition as a function of pressure, temperature and chemical activity. Journal of Sedimentary Petrology 55: 541-547.

Walker, T.R., Waugh, B., Grone, A.J. (1978). Diagenesis in first cycle desert alluvium of Cenozoic age, Southwest United States and Northwest Mexico. American Association of Petroleum Geologists Bulletin 89: 19-32.

Wang, W., Lin, C., Zhang, X. et al. (2020). Effect of burial history on diagenetic and reservoir-forming process of the Oligocene sandstone in Xihu sag, East China Sea Basin. Journal of Marine and Petroleum Geology 112: 1-23.

Welton, J.E. (1984). SEM Petrology Atlas. Volume 4 of American Association of Petroleum Geologists: AAPG methods in exploration series, Issue 4 of methods in exploration series, American Association of Petroleum Geologists.

Wood, J.R. (1989) Modeling the effect of compaction and precipitation/dissolution on porosity. In: Hutcheon. I.E. (ed.) Burial Diagenesis. Mineral Association of Canada Short Course 15: 311-362.